IEEE Access
Multidisciplinary | Rapid Review | Open Access Journal

Received August 1, 2018, accepted September 20, 2018, date of publication September 28, 2018, date of current version October 19, 2018.

Digital Object Identifier 10.1109/ACCESS.2018.2872495

A Dielectric Resonator Antenna-in-Package Design and Its Electromagnetic Interference Investigation on Amplifier

SHENG-JIE GUO[1], (Student Member, IEEE), KWOK WA LEUNG[2,3], (Fellow, IEEE), JUN-FA MAO[1], (Fellow, IEEE), AND NAN YANG[2,3]

[1]Key Laboratory of Ministry of Education of Design and Electromagnetic Compatibility of High Speed Electronics Systems, Shanghai Jiao Tong University, Shanghai 200240, China
[2]State Key Laboratory of Millimeter Waves and the Department of Electronic Engineering, City University of Hong Kong, Hong Kong
[3]Information and Communication Technology Centre, City University of Hong Kong Shenzhen Research Institute, Shenzhen 518057, China

Corresponding author: Kwok Wa Leung (eekleung@cityu.edu.hk)

This work was supported by the National Natural Science Foundation of China/Research Grants Council Joint Research Project under Project N_CityU134/13 and Project 61361166010.

ABSTRACT A highly shielded and easy-integration antenna-in-package (AiP) configuration based on the rectangular hollow dielectric resonator antenna (DRA) is presented. The surfaces of the hollow are made conductive to form a metal cavity, isolating the DRA from the RF circuits. Both passive and active antennas for 2.4-GHz WLAN applications are designed, measured, and compared. The two antennas are excited in the $TE^{x}_{\delta 11}$ mode and perform similarly. To know the effect of the perfect-electric-conductor (PEC) boundary, the DRA without any metal cavities is also studied for comparison. Two sets of experiments are designed to investigate the electromagnetic interference between the AiP and a low-noise amplifier (LNA) inside the hollow. The influences of the DRA on the packaged LNA are measured and analyzed for both the no-PEC-boundary and PEC-boundary cases. It is found that the output of the LNA will be significantly affected by the DRA input power when the latter is sufficiently high.

INDEX TERMS Antenna-in-package (AiP), active integrated antenna (AIA), amplifier, dielectric resonator antenna (DRA), electromagnetic interference (EMI).

I. INTRODUCTION

In recent years, the needs for highly compact and integrated modules are in great demand, including both passive and active designs. The Antenna-in-Package (AiP) as a prospective solution of integrating antennas with RF circuits in a package has been widely studied [1]–[4]. Some novel AiPs realized by low temperature co-fired ceramic (LTCC) technology for RF package applications were designed to operate in 5-GHz band [5]–[7]. According to the relative position of the radio die and antenna, two basic architectures, namely the horizontal and vertical stacking topologies, have been considered in these solutions [8]. An internal-external architecture in [9] provides us a third way for the AiP design.

In 1983, Long *et al.* [10] demonstrated that the dielectric resonator (DR) can be used as an antenna, known as the dielectric resonator antenna (DRA). Since then, the DRA has received much attention because of its low cost, light weight, and high efficiency. The multifunctional DRA has also been extensively explored by making use of its various resonant modes. For example, a single cylindrical DR has been simultaneously designed as an antenna and filter by using its different modes [11]. A triple band cylindrical DRA with three different radiating modes is explored using a novel feeding method [12]. The integration of the DRA with an amplifier or oscillator has also been demonstrated in [13] and [14] to obtain an active integrated antenna (AIA). In [15], a hollow DRA has been used as a package cover for RF circuits, giving an AiP. Although a metal cavity was used to isolate the DRA from the RF chip in [15], the near field of the antenna still influences the chip through the feeding aperture at the top of the cavity, which may cause an electromagnetic interference (EMI) in the system integration.

In an on-chip antennas integrated RF system, active and passive devices are very susceptible to the coupling from antennas [16]. Therefore, the EMI between the RF circuit and antenna should be studied and avoided [17].

Tianwei *et al.* [16] have analyzed and measured the coupling between an on-chip antenna and an inductor. A self-shielded AiP based on the quarter mode substrate-integrated-waveguide (SIW) subarray has been presented in [18]. The electric field inside an AiP structure has been weakened by arranging the via holes properly [19]. However how and what level of the near field will have an influence on chip have not been mentioned. A few studies have been done to investigate the coupling between the AiP and RF circuits [20].

In this paper, a new AiP configuration based on the rectangular hollow DRA is designed. Its feeding probe and hollow for the RF circuits are separated. A second version that has a metallic material on the boundary of the hollow is also investigated. Because of the metallic material, the hollow becomes a cavity. It will be assumed that the metallic material is a perfect electric conductor (PEC). In this version, the antenna and RF circuit can be effectively isolated from each other, minimizing the interference between them and facilitating the integration of high-density and high-sensitivity RF circuits. As a result, the antenna and circuit parts can be designed individually and then connected directly. To illustrate our idea, both passive and active rectangular hollow DRAs working in their fundamental modes are designed, fabricated, and measured in 2.4-GHz band. The active AiP is realized by integrating the passive DRA with power amplifiers.

To study the effect of the PEC cavity and the influence of the antenna's near field on amplifier, two reference antennas (with and without active circuits) that have no PEC boundaries are designed, compared, and discussed. The influence of the AiP on a low noise amplifier (LNA) packaged in its hollow is investigated. To do this, the input-output characteristics of the LNA at different DRA input powers are measured in both cases (with and without the PEC boundary). The impact of the DRA on the gain and DC current of the LNA are studied. The shielding effect of the presented PEC cavity is proved through measurement. While for the no-PEC-boundary case, the influence of the high-power antenna's near field on the active circuit (LNA) is studied, which helps to understand the EMI issue between the AiP and packaged circuits. Finally, the isolations between the DRA and LNA for both cases are measured and compared over 2-3 GHz.

II. ANTENNA-IN-PACKAGE (AIP) DESIGN

A. ANTENNA CONFIGURATION

Fig. 1 shows the AiP configuration. The DRA with a dielectric constant of ε_{ra} has a length of a, width of b, and height of h. It is excited in its $\mathrm{TE}^{x}_{\delta 11}$ mode ($0 < \delta < 1$) by a probe displaced at a distance of d_p from a side wall of the DRA. The length and radius of the probe are l_p and r_p, respectively. A hollow with a length a_1, width of b_1, and height of h_1 is reserved for packaging RF circuits. It is fabricated in the DRA with a distance of d_h from the side wall of the DRA. The AiP is mounted on a square substrate that has a length of G_a, dielectric constant of ε_{rs}, and thickness of t.

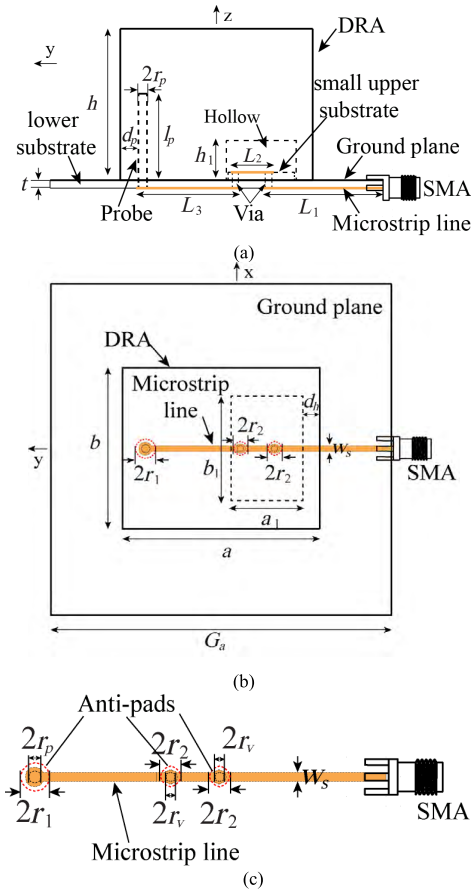

FIGURE 1. Configuration of hollow DRA for AiP: (a) Side view. (b) Top view. (c) Anti-pads.

As shown in the configuration, RF circuits (replaced by a microstrip line with a length of L_2 here) can be placed in the hollow. After the RF circuits have been mounted inside the hollow, they can be connected to the two 50-Ω microstrip lines on the other side of the substrate through via holes (with a radius of r_v). The two microstrip lines with lengths of L_1 and L_3 are connected to the SMA and probe, respectively. In addition, three anti-pads with radii of r_1 and r_2 around the probe and two via holes are etched on the ground plane. All these parameters are optimized to match the antenna at around 2.45 GHz using ANSYS HFSS.

B. DESIGN PARAMETERS

Based on the basic configuration, two antennas with and without the PEC boundaries are optimized and compared in this part. Namely, the difference between them is whether the five walls (four side walls and the top wall) of the hollow inside the DRA have a PEC boundary (metal cavity). To begin with, a displaced-probe-fed rectangular *solid* DRA is designed to resonate in its fundamental $\mathrm{TE}^{x}_{\delta 11}$ mode at around 2.45 GHz [21]. Next, a hollow is fabricated to package the RF circuits. It leads to an increase of the resonant frequency due to the decrease of the equivalent dielectric constant, but it was found that it increases to a smaller

extent when introducing the PEC boundary. To restore the resonant frequency to 2.45 GHz, the sizes of the two DRAs are increased, with the no-PEC-boundary DRA being larger than the PEC-boundary DRA. For convenience, the no-PEC-boundary DRA and PEC-boundary DRA are named as Antenna 1 and Antenna 2, respectively. Their optimized parameters are given in Tables 1 and 2.

TABLE 1. Design parameters of antenna 1.

a	b	h	a_1	b_1	h_1	d_h
29 mm	24.6 mm	19.3 mm	10.5 mm	16.0 mm	5.0 mm	2.5 mm
l_p	d_p	t	G_a	r_p	r_v	r_1
11.0 mm	3.4 mm	0.63 mm	40 mm	0.65 mm	0.5 mm	1.6 mm
r_2	W_s	L_1	L_2	L_3	ε_{ra}	ε_{rs}
1.1 mm	0.92 mm	32.75 mm	6.2 mm	15.35 mm	10	6.5

TABLE 2. Design parameters of antenna 2.

a	b	h	a_1	b_1	h_1	d_h
27.7 mm	23.4 mm	18.5 mm	10.5 mm	16.0 mm	5.0 mm	2.5 mm
l_p	d_p	t	G_a	r_p	r_v	r_1
9.8 mm	3.2 mm	0.63 mm	40 mm	0.65 mm	0.5 mm	1.5 mm
r_2	W_s	L_1	L_2	L_3	ε_{ra}	ε_{rs}
1.1 mm	0.92 mm	33.1 mm	6.2 mm	14.55 mm	10	6.5

C. SIMULATED AND MEASURED RESULTS

Using the optimized dimensions, the two passive antennas were fabricated and measured. In this paper, the reflection coefficients were measured using an Agilent network analyzer 8753ES, whereas the radiation patterns, realized antenna gain, and total efficiencies (mismatch included) of the antennas were measured with a Satimo StarLab system. The fabricated prototypes are shown in Fig. 2.

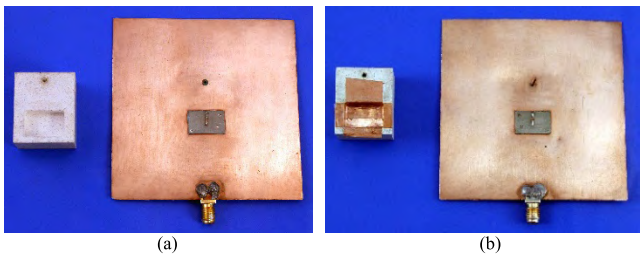

(a) (b)

FIGURE 2. Photos of fabricated prototypes. (a) No-PEC-boundary DRA (Antenna 1). (b) PEC-boundary DRA (Antenna 2).

Fig. 3(a) and Fig. 3(b) show the reflection coefficients of Antenna 1 and Antenna 2, respectively. With reference to Fig. 3(a), the measured impedance bandwidth ($|S_{11}| \leq -10$ dB) of Antenna 1 is 11.3% (2.33-2.61 GHz), which agrees reasonably well with the simulated result of 12.3%

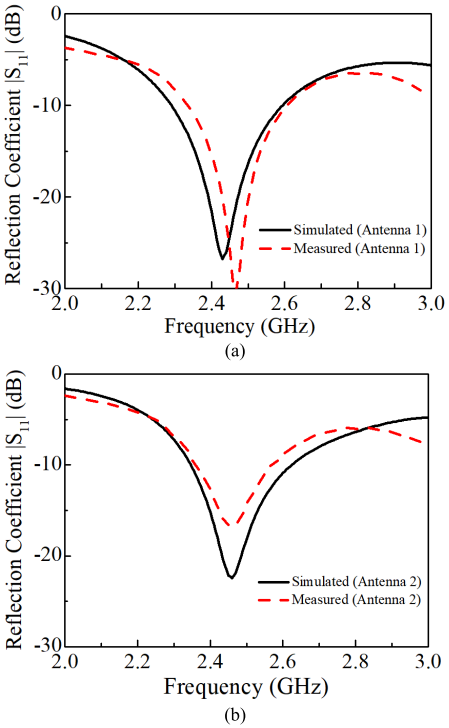

FIGURE 3. Measured and simulated reflection coefficients. (a) No-PEC-boundary DRA (Antenna 1). (b) PEC-boundary DRA (Antenna 2).

(2.29-2.59 GHz). For Antenna 2 (Fig. 3(b)), the measured and simulated bandwidths are 8.9% (2.36–2.58 GHz) and 10.9% (2.35–2.62 GHz), respectively. In both cases, the impedance bandwidths are more than sufficient for 2.4-GHz applications. The deviation between the simulation and measurement is due to fabrication tolerances and experimental imperfections.

Fig. 4 displays the measured and simulated normalized radiation patterns of the two DRAs at 2.45 GHz. A good agreement can be observed for each case. In the boresight direction ($\theta = 0°$), the co-polar field is higher than the cross-polar field by more than 20 dB. A tilting angle of $\sim 10°$ can be found in the E-plane results of the two DRAs because the structure is asymmetry in the E-plane.

The simulated and measured realized antenna gains (mismatch included) of the two DRAs in the boresight direction are shown in Fig. 5. Again, it can be observed from the figure that reasonable agreement is obtained for each antenna. The measured realized gain of Antenna 1 is higher than 4.40 dBi over the 10-dB impedance bandwidth (2.33–2.61 GHz), with the maximum gain being 5.28 dBi at 2.48 GHz. For Antenna 2, the measured realized gain is higher than 4.30 dBi across the 10-dB impedance passband (2.36–2.58 GHz), with the peak gain given by 4.95 dBi at 2.44 GHz. With reference to the figures, the discrepancies between the measured and simulated results are less than 0.77 dB and 0.35 dB for Antenna 1 and Antenna 2, respectively.

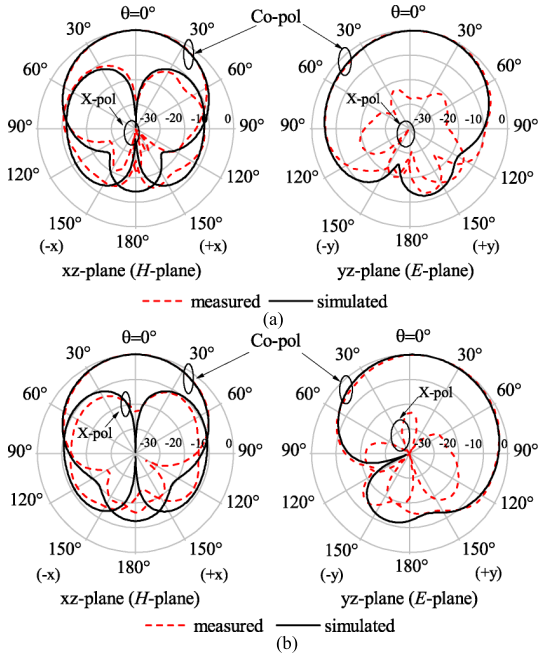

FIGURE 4. Measured and simulated normalized radiation patterns at 2.45 GHz. (a) No-PEC-boundary DRA (Antenna 1). (b) PEC-boundary DRA (Antenna 2).

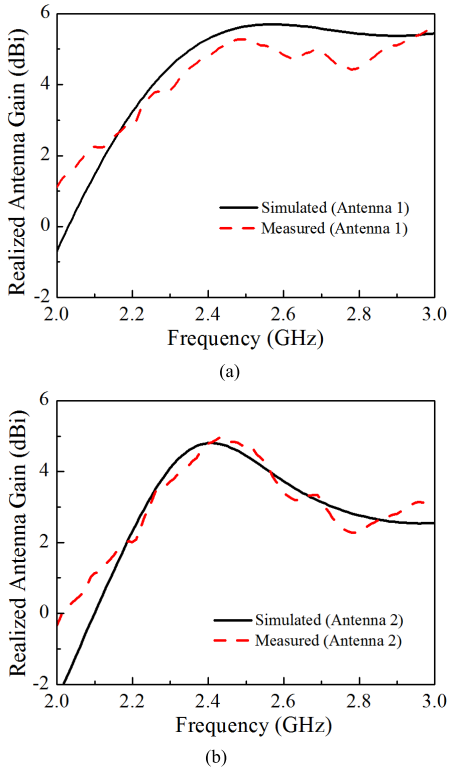

FIGURE 5. Measured and simulated realized antenna gain. (a) No-PEC-boundary DRA (Antenna 1). (b) PEC-boundary DRA (Antenna 2).

Fig. 6 shows the total antenna efficiencies (mismatch included) measured using the Satimo StarLab system. With reference to the figure, the total efficiencies of

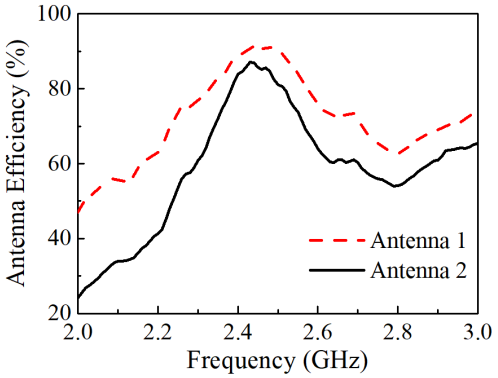

FIGURE 6. Measured total efficiencies (mismatch included) of Antennas 1 and 2.

Antennas 1 and 2 are higher than 77% and 69%, respectively, with their respective maximum efficiencies given by 91% and 87% at 2.45 GHz. A little lower efficiency of Antenna 2 should be mainly due to the roughness of the copper sticker that forms the PEC boundary of the hollow.

III. ACTIVE INTEGRATED ANTENNA (AIA) DESIGN

An AIA or system-in-package can be easily realized using our AiP configuration. For demonstration, two AIAs using Antennas 1 and 2 were designed, fabricated, and measured.

A. CONFIGURATION OF THE AIAs

The configuration of our AIAs with or without the PEC boundary is shown in Fig. 7. The designs without and with the PEC boundary are denoted as AIA 1 and AIA 2, respectively. Here, the two hollow DRAs are based on the passive designs in Fig. 1.

A Mini-Circuits GALI-S66+ [22] amplifier is used for both AIAs 1 and 2. The amplifier is internally matched to 50 ohm and only some blocking capacitors and bias circuits are needed. According to the recommended evaluation board [22], the circuit topology of the amplifier was designed on a $15.5 \times 10 \times 0.63$ mm^3 substrate with a dielectric constant of $\varepsilon_{rs} = 6.15$, as shown in Fig. 7(b).The amplifier is connected to two microstrip line sections through via holes; one of the section is connected to the SMA connector whereas the other section is connected to a feeding probe.

B. PERFORMANCE OF THE AIAs

Two prototypes of the proposed AIAs were fabricated, with their photos shown in Fig. 8. To show the structures clearly, they are unassembled in the figures and the PA part is magnified in Fig. 8(c) to see the details well.

The measured reflection coefficients with the DC power supply applied are displayed in Fig. 9. Since the input impedance of the amplifier is unavailable in the datasheet, the simulated reflection coefficients of the two AIAs are not included in the figure. In the measurements, the amplifier was fed by an input of −30 dBm. The measured 10-dB impedance bandwidths of AIAs 1 and 2 are 2.38−2.80 GHz

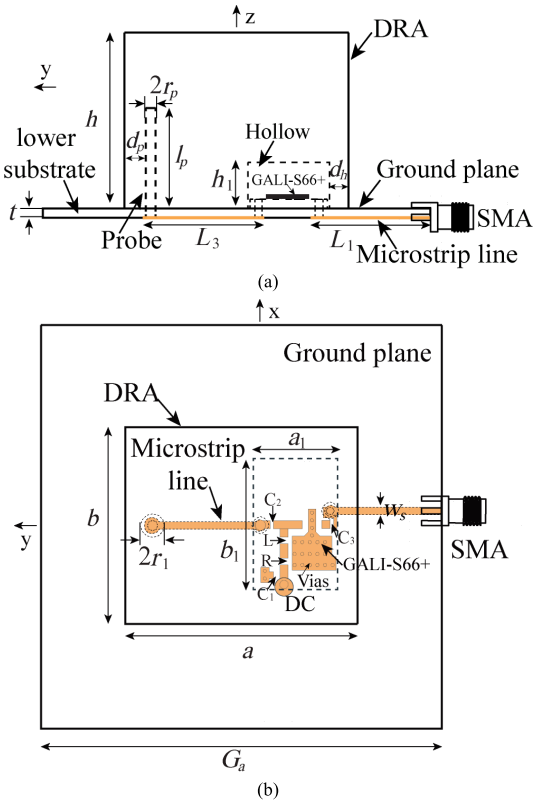

FIGURE 7. Configuration of AIAs with or without PEC boundary: R = 499 Ω, C1 =0.1 μF, C2 = C3 = 2400 pF, and L = 22 nH. The DC voltage is 12 V. (a) Side view. (b) Top view.

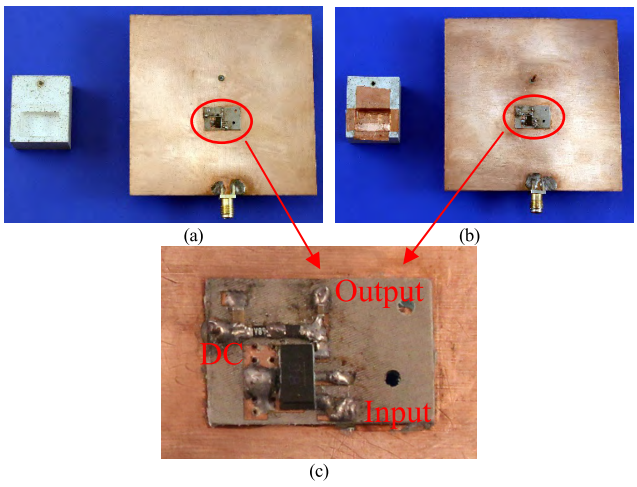

FIGURE 8. Photos of two AIA prototypes. (a) No-PEC-boundary AIA (AIA 1). (b) PEC-boundary AIA (AIA 2). (c) The magnified PA in both AIAs.

and 2.29−2.78 GHz, respectively. Both of them fully cover the 2.4-GHz WLAN band.

Fig. 10 shows the measured normalized radiation patterns of the two AIAs at 2.45 GHz. As compared with the simulated radiation patterns of the passive counterpart (Fig. 4(a)), reasonable agreement between the measured and simulated results can be observed. The cross-polar field of AIA 1 deteriorates a little bit but is still lower than the co-polar field by

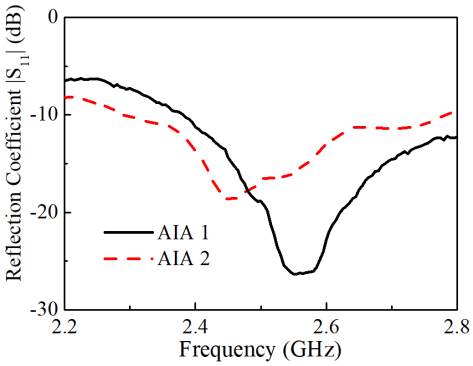

FIGURE 9. Measured reflection coefficients of AIA 1 (without PEC boundary) and AIA 2 (with PEC boundary). The parameters are the same as in Tables 1 and 2.

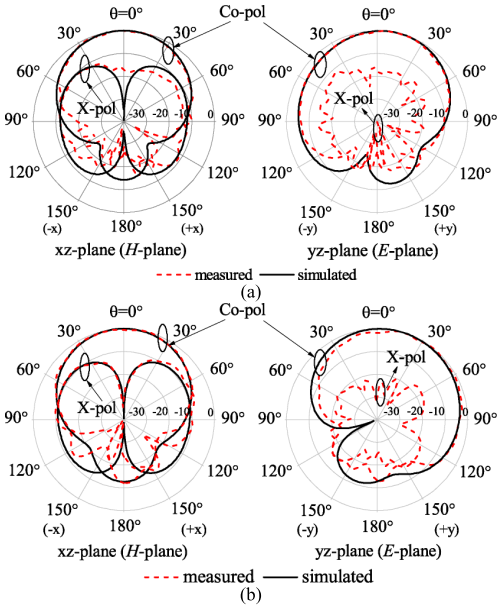

FIGURE 10. Measured and simulated normalized radiation patterns at 2.45 GHz. (a) No-PEC-boundary AIA (AIA 1). (b) PEC-boundary AIA (AIA 2).

at least 15 dB, being enough for many practical applications. The deterioration of the cross-polar field should be mainly due to the mutual coupling between the antenna and amplifier. In contrast, AIA 2 can suppress the cross-polar field to lower than −20 dB because the amplifier is isolated by the PEC boundary. Thus, the PEC boundary should be used in most applications to reduce undesirable cross-polar fields.

Theoretically, the realized gains of the AIAs can be obtained by adding the simulated gains of the passive DRAs (Antennas 1 and 2) and the typical gain of the amplifier (∼17.5 dB at 2.4 GHz). Fig. 11 compares the measured and theoretical realized gains of the two AIAs in the boresight direction. As can be seen from Fig. 11, the measured realized gains of AIAs 1 and 2 over the 2.4-GHz band are higher than 22 and 21 dBi, respectively. For both AIAs, the measured and theoretical results are in reasonable agreements, with the deviations being less than 1.3 dB.

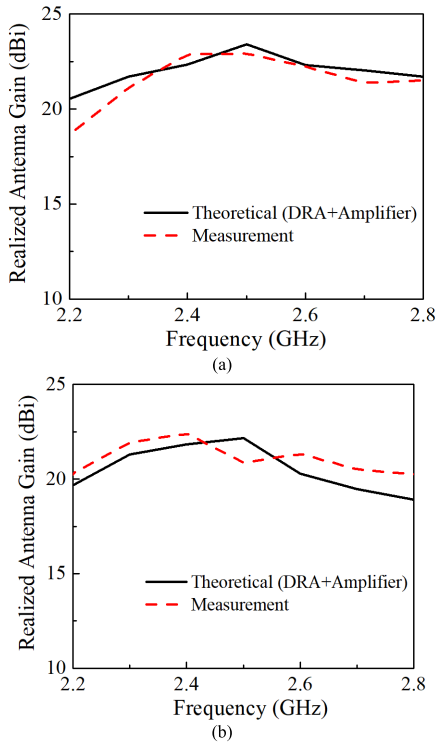

FIGURE 11. Measured and theoretical gains of two AIAs. The theoretical gain is the sum of the DRA gain and amplifier gain. (a) No-PEC-boundary AIA (AIA 1). (b) PEC-boundary AIA (AIA 2).

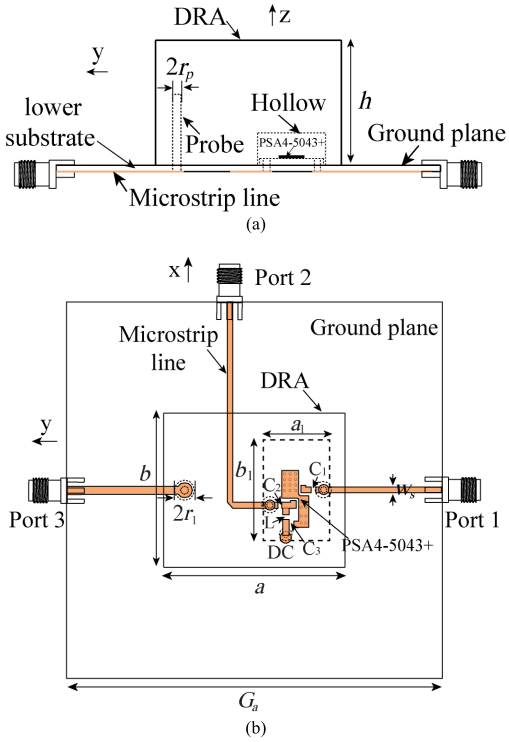

FIGURE 12. Configuration of DRA packaging LNA: C1 = C2 = 1000 pF, C3 = 2400 pF, and L = 22 nH. The DC voltage is 5 V. (a) Side view. (b) Top view.

It should be mentioned that the gains of AIAs 1 and 2 are more or less the same because the input power of the amplifier is not high. As will be demonstrated in the following section, the two AIAs will perform very differently when the input power is high.

IV. EMI INVESTIGATION

Although a PEC cavity or grounded shield is often used to isolate RF circuits from antennas, the effects of the cavity/shield on the antenna radiation and RF circuits have been seldom found. The influence of a high-power external plane-wave EMI on the performance of an RF amplifier via a slot on a cavity has been analyzed and measured in [23]. However, only limited work has been done on studying the coupling and interaction between an AiP and its packaged RF circuits, which is a near-field problem. In this section, two experiments based on our AiP configuration are designed to study the effect of the near field of the antenna on the amplifier. Due to the limitation of the test equipment, the noise figure of the LNA was not measured.

A. TESTING STRUCTURE

The configuration of the testing structure is shown in Fig. 12. With reference to the figure, each hollow DRA in Section II is used to package an amplifier. Since this section is focused on the EMI, higher powers were used in the experiment and therefore a low-noise amplifier (LNA) with a high input 1-dB compression point is used here. A Mini-Circuits

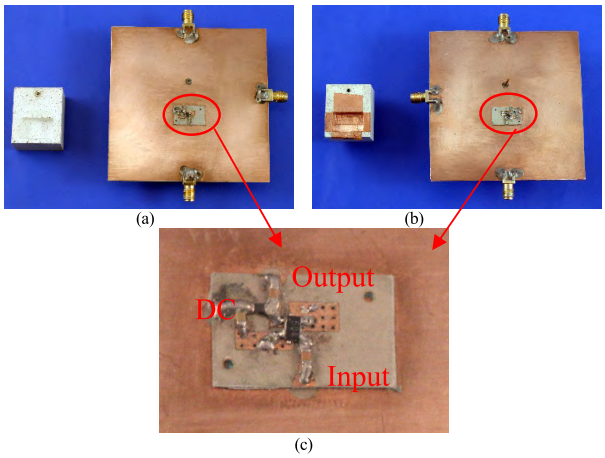

FIGURE 13. Photos of DRA and LNA. (a) No-PEC-boundary case. (b) PEC-boundary case. (c) The magnified LNA in both cases.

PSA4-5043+ [24], which is internally matched, is used as the LNA. A LNA circuit was designed on a $15.5 \times 10 \times 0.63$ mm^3 substrate ($\varepsilon_{rs} = 6.15$) according to the suggested evaluation board [24], as shown in Fig. 12(b). The input port of the DRA (Port 3) and output port of the LNA (Port 2) are connected to two SMA connectors via 50-Ω microstrip lines individually for the EMI investigation. Two sets of experiments (with and without the PEC boundary) were designed at 2.40 GHz. Fig. 13 shows the photos of the unassembled prototypes and the LNA part is magnified in Fig. 13(c) to see the details well.

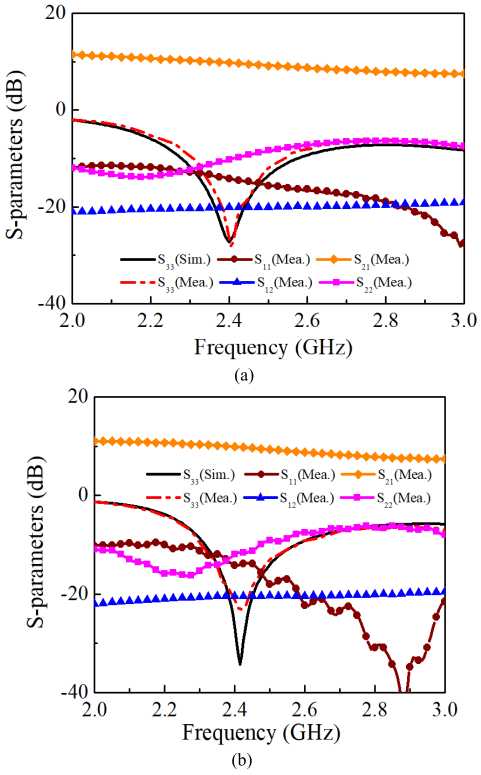

FIGURE 14. Simulated and measured S-parameters of DRAs with LNAs. (a) No-PEC-boundary case. (b) PEC-boundary case.

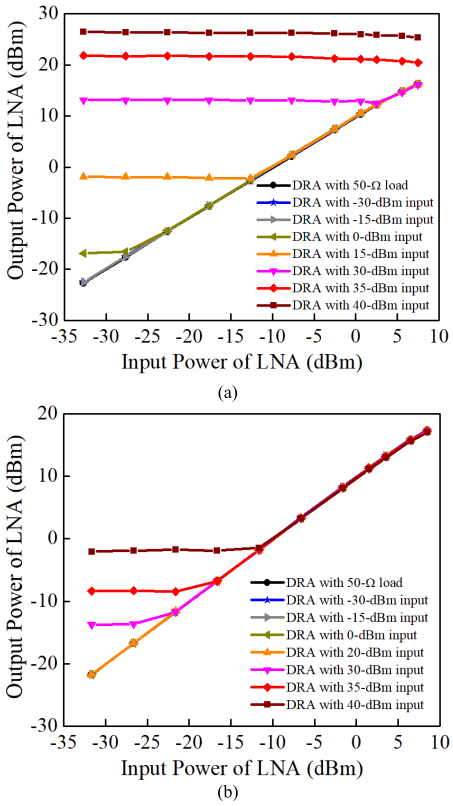

FIGURE 15. Measured input and output of LNA at 2.40 GHz for different DRA input powers. (a) No-PEC-boundary case. (b) PEC-boundary case.

B. S-PARAMETERS OF THE SYSTEMS

Fig. 14 shows the reflection coefficients (S_{11}, S_{22}, and S_{33}) and transmission coefficients (S_{21} and S_{12}) of the two cases. The output power of the network analyzer was set as -20 dBm and the LNA worked in its linear region. It can be seen from the figure that the measured S_{11} of the no-PEC-boundary and PEC-boundary cases are lower than -11.5 dB and -9.5 dB, respectively. For both cases, the matching levels (S_{22}) at the output ports of the LNAs are around -10 dB across the 2.4-GHz band. With reference to the figure, the measured and simulated 10-dB impedance bandwidths ($|S_{33}| < -10$ dB) of the DRA without the PEC boundary are 9.5% (2.31–2.54 GHz) and 12.0% (2.28–2.57 GHz), respectively. For the PEC-boundary case, the measured 10-dB impedance bandwidth starts from 2.30 GHz to 2.58 GHz (11.5%), agreeing well with the simulated bandwidth of 11.0% (2.31–2.58 GHz). Again, both cases can entirely cover the 2.4-GHz WLAN band. It is worth mentioning that the simulated S_{33} in Fig. 14 agrees well with the simulated S_{11} in Fig. 3, implying that the RF circuit does not affect the antenna, as desired. For both cases, the measured gain (S_{21}) and isolation ($-S_{12}$) of the LNAs are about 10 dB and 20 dB respectively.

C. INPUT VS OUTPUT OF THE LNA

Fig. 15 shows the measured input-output characteristic of the LNA at 2.40 GHz for different input powers to the DRA. In the measurements, the input power of the LNA was increased from -32.5 dBm to 7.5 dBm with a step of 5 dB, whereas that of the DRA was increased from -30 dBm to 40 dBm with the same step. The different DRA input corresponds to a different magnitude of the near field inside the hollow. The input-output curve when the DRA is connected to a 50-Ω load was also measured, and the result is given in the figure for comparison. For clarity, only selected cases are shown in the figure. With reference to Fig. 15(a) (no PEC-boundary), when the input power of the DRA is low, say below 0 dBm, the output of the LNA increases linearly with the input power of the LNA at Port 1 as if the DRA did not exist. However, when the input power of the DRA gets higher, the output of the LNA will be affected by the input power of the DRA. For example, when the DRA input power is 15 dBm, an almost constant LNA output power of about -2.0 dBm is found for a LNA input power of below -12.5 dBm. This phenomenon holds when the measured input power of the DRA is higher than 0 dBm. From the many measured data sets (some of them arenot shown in the figure), it can be concluded that the input-output characteristic of the LNA is strongly affected by the DRA when the input power of the DRA is higher than that of the LNA by ∼27 dB or more.

A similar phenomenon can be observed for the PEC-boundary case (Fig. 15(b)) with a different threshold input power to the DRA. It was found from the measurement

that the linear input-output characteristic is not affected by the DRA until the input power of the DRA reaches 22.0 dBm. An analysis of the measurement data shows that the input-output characteristic of the LNA is strongly affected by the DRA when the input power of the DRA is higher than that of the LAN by ∼54 dB or more. This threshold value is 27 dB higher than that of the no-PEC-boundary case, showing that using the PEC can isolate the circuit from the DRA very effectively.

In both cases, for a fixed DRA input (smaller than 30 dBm), when the difference between the inputs of the DRA and LNA is smaller than the threshold value, the output of the LNA are still increasing linearly with the LNA input, namely the LNA is working normally for these cases. It implies that for this fixed DRA input, the LNA output is directly influenced by the DRA's coupling, whereas the working state (gain) of the LNA is nearly not affected, which will be further verified by the unchanged DC current part in Subsection E.

D. GAIN OF THE LNA

It has been found in [23] that a plane-wave EMI at a power of 23 dBm can cause the gain of an RF power amplifier to degrade by ∼8 dB by changing its DC current and working state. In this part, the effect of the antenna's near field on the LNA gain is studied. Only low input powers of the DRA are considered in this part. It is because when the DRA input power is high, the output of the LNA will be seriously affected and the LNA output will not be simply equal to the LNA input multiplied by the LNA gain. Fig. 16 shows the LNA gain (output power divided by input power) as a function of the LNA input power for different DRA input powers. As can be observed from the figure, the LNA gain is ∼10 dB in the linear region regardless of having a PEC boundary or not. The input 1-dB compression point is ∼5.5 dBm for both the no-PEC-boundary and PEC-boundary cases. However, it can be observed that the gain varies with different antenna inputs for the no-PEC-boundary case, with the maximum difference being 0.2 dB. In contrast, the gain remains almost the same for the PEC-boundary case for different DRA input powers. In other words, the PEC boundary desirably helps stabilize the gain of the LNA.

E. DC CURRENT OF THE LNA

Fig. 17 shows the measured DC current of the LNA as a function of the LNA input for different DRA input powers. With reference to the figure, as the input power of the LNA increases, the DC current initially remains at ∼50 mA and then increases with the LNA input. It can be expected because normally the DC current will not vary significantly until the working state of the LNA changes from the linear region to the nonlinear region. The change of the working state can also be seen from the gain compression in Fig. 16.

It is observed that when there is no PEC boundary (Fig. 17(a)), the DC current changes at a lower LNA input as the input of DRA increases to larger than 30 dBm. But when the input power of the DRA is high (such as 40 dBm), the current becomes totally different. In this case, the current starts from 62.5 mA and varies between 59 mA and 64 mA. This phenomenon can be explained by the fact that a high voltage can be induced by the near field of the DRA when there is no PEC boundary [25], altering the equivalent DC voltage. In contrast, when a PEC boundary is used (Fig. 17(b)), the current remains virtually unchanged for different DRA inputs. Obviously, using a PEC boundary in an AiP can give better results.

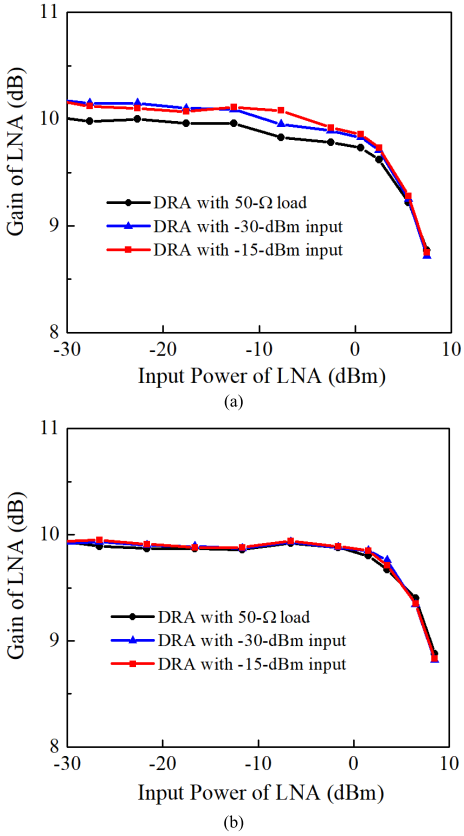

FIGURE 16. Measured gains of the LNA at 2.40 GHz for different DRA input powers. (a) No-PEC-boundary case. (b) PEC-boundary case.

F. COUPLING BETWEEN THE LNA AND DRAs

It has been shown in Part C that it starts to affect the output of the LNA significantly when the DRA input is higher than the LNA input by 27 dB and 54 dB for the no-PEC-boundary and PEC-boundary cases, respectively. These threshold values are valid for 2.40 GHz only. This part is to study the threshold values over the frequency range of 2-3 GHz. For simplicity, the LNA input was fixed at −32.5 dBm in the measurement, and the DRA input was gradually increased from −30 dBm until the output of LNA changed. The input power of the DRA can be used to obtain the threshold values by simply subtracting the DRA input by the LNA input (−32.5 dBm).

The calculated threshold values for the no-PEC-boundary and PEC-boundary cases are both shown in Fig. 18 for ease of comparison. As can be seen from the figure, when the hollow has no PEC boundary, the threshold value is ∼30 dB

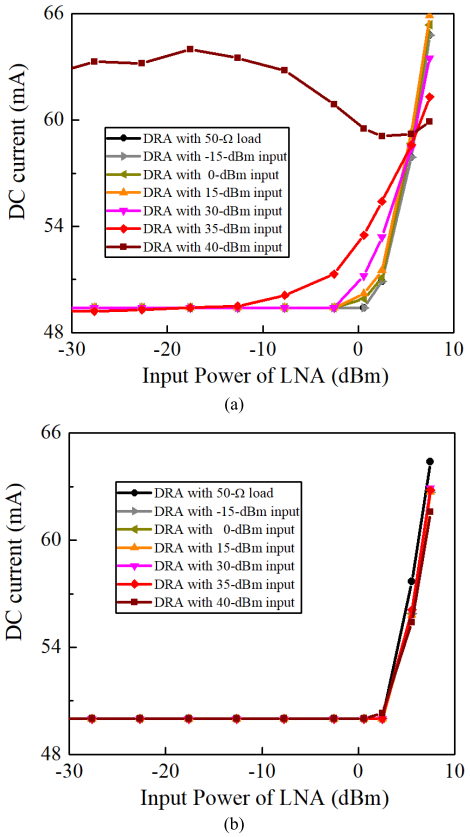

FIGURE 17. Measured DC current of the LNA at 2.40 GHz for different DRA input powers. (a) No-PEC-boundary case. (b) PEC-boundary case.

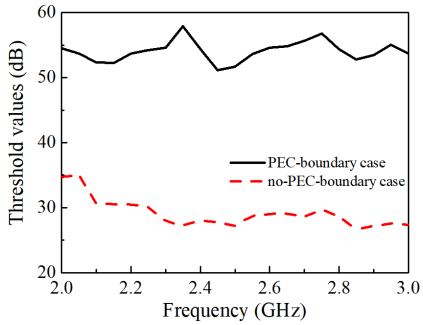

FIGURE 18. Measured threshold values. (a) No-PEC-boundary case. (b) PEC-boundary case.

over the frequency range of 2-3 GHz. This value can be very challenging for high-gain, high-sensitivity RF systems. But when the PEC boundary is used, the threshold value is higher than 50 dB, which is 25 dB more than that of the no-PEC-boundary case. The result is very favorable.

V. CONCLUSION

A new configuration of rectangular DRA with a shielded hollow has been presented for AiP designs. Two passive AiPs, with and without the PEC boundary, have been designed first to study their antenna performances. Their measured 10-dB impedance bandwidths have been found to be 11.3% (2.33–2.61 GHz) and 8.9% (2.36–2.58 GHz) for no-PEC-boundary and PEC-boundary cases, respectively, entirely covering 2.4-GHz WLAN band. It has been observed that their measured radiation patterns agree reasonably well with the simulated results, with their realized gains being higher than 4.30 dBi. Two RF amplifiers have been integrated inside the hollow of the DRAs. The measured S-parameters and realized antenna gains of the two AIAs are similar, regardless of having a PEC boundary or not. However, it has been found that the cross-polar field of the PEC-boundary case is desirably much weaker than that of no-PEC-boundary case.

The EMI issue has also been addressed. The hollow DRAs and their packaged LNAs have been separated and connected to different ports, forming two three-port systems (Fig. 12). It has been found that the coupling of the DRA affects the output of the LNA severely. It has been observed that to operate the LNA normally, the input powers of the DRAs should not be higher than those of the LNA by the threshold values. The influence mechanism of the antenna's near field on the performance of the active circuit (LNA) is analyzed. It has been shown that by using the PEC boundary, the threshold value can be increased by ∼25 dB over the frequency range of 2-3 GHz. Also, the operation and performance of the LNA can be more stable.

ACKNOWLEDGMENT

The authors would like to thank Mr. M. S. Leung for taking the photos.

REFERENCES

[1] Y. P. Zhang, "Integration of microstrip patch antenna on ceramic ball grid array package," *Electron. Lett.*, vol. 38, no. 5, pp. 207–208, Feb. 2002.
[2] U. Ullah, N. Mahyuddin, Z. Arifin, M. Z. Abdullah, and A. Marzuki, "Antenna in LTCC technologies: A review and the current state of the art," *IEEE Antennas Propag. Mag.*, vol. 57, no. 2, pp. 241–260, Apr. 2015.
[3] C. W. Ling, C. Y. Lee, C. L. Tang, and S. J. Chung, "Analysis and application of an on-package planar inverted-F antenna," *IEEE Trans. Antennas Propag.*, vol. 55, no. 6, pp. 1774–1780, Jun. 2007.
[4] Y. P. Zhang, "Enrichment of package antenna approach with dual feeds, guard ring, and fences of vias," *IEEE Trans. Adv. Packag.*, vol. 32, no. 3, pp. 612–618, Aug. 2009.
[5] S. H. Wi *et al.*, "Package-level integrated LTCC antenna for RF package application," *IEEE Trans. Adv. Packag.*, vol. 30, no. 1, pp. 132–141, Feb. 2007.
[6] Y. P. Zhang, M. Sun, and W. Lin, "Novel antenna-in-package design in LTCC for single-chip RF transceivers," *IEEE Trans. Antennas Propag.*, vol. 56, no. 7, pp. 2079–2088, Jul. 2008.
[7] L. Li, X. Chen, Y. Zhang, L. Han, and W. Zhang, "Modeling and design of microstrip patch antenna-in-package for integrating the RFIC in the inner cavity," *IEEE Antennas Wireless Propag. Lett.*, vol. 13, pp. 559–562, 2014.
[8] Y. P. Zhang and D. Liu, "Antenna-on-chip and antenna-in-package solutions to highly integrated millimeter-wave devices for wireless communications," *IEEE Trans. Antennas Propag.*, vol. 57, no. 10, pp. 2830–2841, Oct. 2009.
[9] A. P. Popov, M. D. Rotaru, and M. K. Lyer, "Packaged integrated antenna for circular and linear polarizations," U.S. Patent 6 879 287 B2, Apr. 12, 2005.
[10] S. A. Long, M. McAllister, and L. Shen, "The resonant cylindrical dielectric cavity antenna," *IEEE Trans. Antennas Propag.*, vol. AP-31, no. 3, pp. 406–412, May 1983.
[11] L. K. Hady, D. Kajfez, and A. A. Kishk, "Dielectric resonator antenna in a polarization filtering cavity for dual function applications," *IEEE Trans. Microw. Theory Techn.*, vol. 56, no. 12, pp. 3079–3085, Dec. 2008.
[12] A. Sharma, G. Das, P. Ranjan, N. K. Sahu, and R. K. Gangwar, "Novel feeding mechanism to stimulate triple radiating modes in cylindrical dielectric resonator antenna," *IEEE Access*, vol. 4, pp. 9987–9992, 2016.

[13] M. G. Keller, D. J. Roscoe, M. B. Oliver, R. K. Mongia, Y. M. M. Antar, and A. Ittipiboon, "Active aperture-coupled rectangular dielectric resonator antenna," *IEEE Microw. Guided Wave Lett.*, vol. 5, no. 11, pp. 376–378, Nov. 1995.
[14] E. H. Lim and K. W. Leung, "Novel utilization of the dielectric resonator antenna as an oscillator load," *IEEE Trans. Antennas Propag.*, vol. 55, no. 10, pp. 2686–2691, Oct. 2007.
[15] E. H. Lim and K. W. Leung, "Novel application of the hollow dielectric resonator antenna as a packaging cover," *IEEE Trans. Antennas Propag.*, vol. 54, no. 2, pp. 484–487, Feb. 2006.
[16] T. Deng, Z. Chen, and Y. P. Zhang, "Coupling mechanisms and effects between on-chip antenna and inductor or coplanar waveguide," *IEEE Trans. Electron Devices*, vol. 60, no. 1, pp. 20–27, Jan. 2013.
[17] T. Sudo, H. Sasaki, N. Masuda, and J. L. Drewniak, "Electromagnetic interference (EMI) of system-on-package (SOP)," *IEEE Trans. Adv. Packag.*, vol. 27, no. 2, pp. 304–314, May 2004.
[18] C. Jin, R. Li, S. Hu, S. Zhang, K. F. Chang, and B. Zheng, "Self-shielded circularly polarized antenna-in-package based on quarter mode substrate integrated waveguide subarray," *IEEE Trans. Compon., Packag., Manuf. Technol.*, vol. 4, no. 3, pp. 392–399, Mar. 2014.
[19] G. Han, J. Yang, X. Chen, Y. Geng, Y. Zhang, and W. Zhang, "Study on the near field characteristic of antenna in package," *IEEE Trans. Compon., Packag. Manuf. Technol.*, vol. 2, no. 9, pp. 1449–1454, Sep. 2012.
[20] K.-K. Huang and D. D. Wentzloff, "A 60 GHz antenna-referenced frequency-locked Loop in 0.13μm CMOS for wireless sensor networks," *IEEE J. Solid-State Circuits*, vol. 46, no. 12, pp. 2956–2965, Dec. 2011.
[21] X. S. Fang, C. K. Chow, K. W. Leung, and E. H. Lim, "New single-/dual-mode design formulas of the rectangular dielectric resonator antenna using covariance matrix adaptation evolutionary strategy," *IEEE Antennas Wireless Propag. Lett.*, vol. 10, pp. 734–737, 2011.
[22] *The Datasheet of GALI-S66 can be Found at Mini-Circuits*. Accessed: Sep. 29, 2018. [Online]. Available: https://www.minicircuits.com/WebStore/dashboard.html?model=GALI-S66%2B
[23] Y. Bayram, J. L. Volakis, S. K. Myoung, S. J. Doo, and P. Roblin, "High-power EMI on RF amplifier and digital modulation schemes," *IEEE Trans. Electromagn. Compat.*, vol. 50, no. 4, pp. 849–860, Nov. 2008.
[24] *The Datasheet of PSA4-5043+ can be Found at Mini-Circuits*. Accessed: Sep. 29, 2018. [Online]. Available: https://www.minicircuits.com/WebStore/dashboard.html?model=PSA4-5043%2B
[25] T. Yang, T. Bayram, and J. L. Volakis, "Hybrid analysis of electromagnetic interference effects on microwave active circuits within cavity enclosures," *IEEE Trans. Electromagn. Compat.*, vol. 52, no. 3, pp. 745–748, Aug. 2010.

SHENG-JIE GUO (S'13) was born in Zhoukou, Henan, China. He received the B.Eng. degree from the School of Electronic Engineering, Xidian University, Xi'an, China, in 2013. He is currently pursuing the Ph.D. degree in electronic science and technology with Shanghai Jiao Tong University, Shanghai, China. His current research interests include dielectric resonator antenna, antenna in package, and electromagnetic compatibility in the system-in-package design.

KWOK WA LEUNG (S'90–M'93–SM'02–F'11) was born in Hong Kong. He received the B.Sc. degree in electronics and the Ph.D. degree in electronic engineering from The Chinese University of Hong Kong, Hong Kong, in 1990 and 1993, respectively. In 1994, he joined the Department of Electronic Engineering, City University of Hong Kong (CityU), Hong Kong, where he is currently a Chair Professor and also the Founding Director of the Innovation Centre of the Department. In 2006, he was a Visiting Professor with the Department of Electrical Engineering, Pennsylvania State University, State College, PA, USA. His research interests include RFID tag antennas, dielectric resonator antennas, microstrip antennas, wire antennas, guided wave theory, computational electromagnetics, and mobile communications.

Dr. Leung is a member of the IEEE AP-S Distinguished Lecturer Committee. He was a recipient of the International Union of Radio Science Young Scientists Awards in Kyoto, Japan and St. Petersburg, Russia, in 1993 and 1995, respectively. He was also a recipient of the Departmental Outstanding Teacher Awards in 2005, 2010, and 2011 and the CityU Research Excellence Award in 2013. He received the IEEE AP-S Transactions Commendation Certificates twice, in 2009 and 2010, for his exceptional performance. He was the Chairman of the IEEE AP/MTT Hong Kong Joint Chapter for the years of 2006 and 2007. He was the Chairman of the Technical Program Committee, 2008 Asia–Pacific Microwave Conference, Hong Kong, the Co-Chair of the Technical Program Committee, 2006 IEEE TENCON, Hong Kong, and the Finance Chair of PIERS 1997, Hong Kong. He was an Editor of *HKIE Transactions* and a Guest Editor of *IET Microwaves, Antennas, and Propagation*. He was an Associate Editor of the IEEE TRANSACTIONS ON ANTENNAS AND PROPAGATION. He was also an Associate Editor of the IEEE ANTENNAS AND WIRELESS PROPAGATION LETTERS. He is currently the Editor-in-Chief of the IEEE TRANSACTIONS ON ANTENNAS AND PROPAGATION. He was a Distinguished Lecturer of the IEEE Antennas and Propagation Society from 2012 to 2014.

JUN-FA MAO (M'92–SM'98–F'12) was born in 1965. He received the B.S. degree in radiation physics from the University of Science and Technology of National Defense, China, in 1985, the M.S. degree in experimental nuclear physics from the Shanghai Institute of Nuclear Research, Chinese Academy of Sciences, China, in 1988, and the Ph.D. degree in electronic engineering from Shanghai Jiao Tong University, Shanghai, China, in 1992. Since 1992, he has been a Faculty Member with Shanghai Jiao Tong University, where he is currently a Chair Professor and the Dean of the School of Electronic, Information and Electrical Engineering. He was a Visiting Scholar with The Chinese University of Hong Kong, Hong Kong, from 1994 to 1995, and a Post-Doctoral Researcher with the University of California at Berkeley, Berkeley, from 1995 to 1996. He has authored or co-authored more than 250 journal papers (including more than 110 IEEE journal papers) and 140 international conference papers. His research interests include the interconnection and package problem of integrated circuits and systems and analysis and design of microwave components and circuits.

Dr. Mao was a member of the 2015 IEEE Fellow Committee and the 2012–2014 Fellow Evaluation Committee of the IEEE Microwave Theory and Techniques Society. He received the National Natural Science Award of China in 2004, the National Technology Invention Award of China in 2008, the National Science and Technology Advancement Award of China in 2012, and five best paper awards of international conferences. He is a Chief Scientist of the National Basic Research Program (973 program) of China, a Project Leader of the National Science Foundation for Creative Research Groups of China, a Cheung Kong Scholar of the Ministry of Education, China, an Associate Director of the Microwave Society of China Institute of Electronics (CIE), a fellow of CIE, the 2007–2009 Chair of the IEEE Shanghai Section, and the 2009–2016 Chair of the IEEE MTT-S Shanghai Chapter.

NAN YANG was born in Yangling, Shaanxi, China, in 1987. He received the B.Sc. and M.Eng. degrees in electronic engineering from Zhejiang University, Hangzhou, Zhejiang, China, in 2008 and 2012, respectively, and the Ph.D. degree from the City University of Hong Kong, Hong Kong, in 2016. He is currently a Post-Doctoral Fellow with the City University of Hong Kong. His research interests include microwave and mm-wave circuits and dielectric resonator antennas.